Structural damage detection based on quadratic correlation function of strain responses

Miao Li[ab] , Tianli Huang[c]*

[a]School of Civil Engineering, Hunan City University, Yiyang 413000, China. E-mail: lm_hncu@163.com
[b]Hunan Engineering Research Center of Development and Application of Ceramsite Concrete Technology, Hunan City University, Yiyang 413000, China.
[c]Schoolof Civil Engineering, Central South University, Changsha 410075, China. E-mail: htianli@csu.edu.cn

*Corresponding author

Abstract

A damage detection method based on the quadratic correlation function of strain responses (QCoS) and pattern matching degree (PMD) is proposed in the present study. For this method, only QCoS is calculated in time domain by strain responses, and there is no need for modal parameter extraction and analytical model of structures. It is proved that QCoS is the function of modal parameters of structures, such as natural frequency, mode shape and damping ratio. Numerical simulations of a simply supported steel beam are analyzed for illustrating the effect of excitation position, reference point and damage level on QCoS, respectively. The results show that QCoS is sensitive to local damage in the structure and robust to measurement noise. Therefore, QCoSs are used to construct the damage feature vector. The damage detection is performed by comparing the damage feature vectors before and after the structural damage. Three simply supported aluminum beams are tested in the laboratory to demonstrate the effectiveness and practicability of the proposed method.

Keywords

Structrual damage identification, strain responses, quadratic correlation function, pattern matching degree

Graphical Abstract
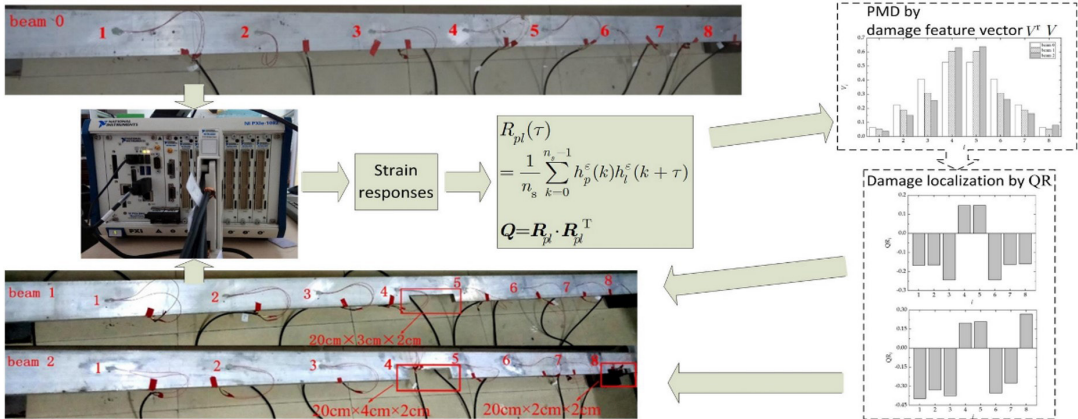
1 INTRODUCTION

During the operation of engineering structures, the local damage to structural components will accumulate due to various factors such as material ageing, environmental corrosion and fatigue loading, and engineering accidents may occur (Peeters and Roeck, 2001; Omenzetter et al., 2004; Deraemaeker et al., 2008). In structural health monitoring, damage identification methods based on structural vibration testing have always been a research hotspot (Gul and Catbas, 2008; Zhang et al., 2022).

The occurrence of structural damage leads to changes in physical parameters, such as structural mass and stiffness, and the modal parameters of the structure change accordingly. Structural damage has been detected by identifying the change in modal parameters such as natural frequencies, mode shapes, and their variants. Salawu (1997) reviewed structural assessment methods based on frequency variation and discussed the relationship between damage and frequency variation. Sha et al. (2019) proposed a two-step method for damage detection in beams based on the relative natural frequency change (RNFC) curves. The method can not only localize but also quantify single and multiple damage, relying only on natural frequencies. De Medeiros et al. (2016; 2018), Medeiros et al. (2021) developed damage indexes that take into account both the amplitude and phase of FRFs, obtained from vibration responses of the structure, to identify damage in composite plates and bonded joints. He et al. (2018) used the Hilbert transform to extract the modal shape with high spatial resolution from acceleration responses of a damaged beam, and proposed the regional mode shape curvature as a damage index to locate damage. Although damage identification methods based on modal parameters have been widely utilized in cilvil engineering structures, the lower-order modes are insensitive to minor structural damage, and higher-order modes are difficult to obtain despite their high sensitivity to structural damage (Huth et al., 2005; Lou et al., 2014; Lu et al., 2017; Shang et al., 2021). To avoid modal identification in damage detection, Yan et al. (2022) developed a new method based on the power spectral density transmissibility function.

Given the limitations of modal-based structural damage detection methods, many researchers have investigated the methods by constructing the damage indicators with structural dynamic responses in the time domain. Nair et al. (2006) established the AR time series model of structural responses and took the model coefficients as damage indicators. Trendafilova and Manoach (2008), Manoach et al. (2012; 2017) directly constructed the damage index by combining displacements and velocity responses of plates and composite beams to detect damage. Rezaei and Taheri (2009) decomposed the vibration response of a cantilevered steel pipe by using empirical mode decomposition (EMD) and used the first-order intrinsic model function (IMF) to realize the damage detection of the pipe. Yang et al. (2019) proposed a model-free structural damage identification method based on the acceleration statistical moment index in the time domain. Through the relative change of the index, the damages of the RC frame structure were quickly diagnosed. Recently, the cross-correlation function of structural responses in damage detection has attracted considerable attention for its high sensitivity to structural damage and noise immunity. Yang et al. (2007), Wang et al. (2010, 2013) took the acceleration cross-correlation function magnitude vector (CorV) as a damage indicator for structural damage detection. The relative difference between the CorVs obtained from intact and damaged structures was used to locate the damage. Li and Law (2010) constructed a damage index based on acceleration auto/cross-correlation function covariance. In comparison to acceleration, strain is more sensitive to variations in the local stiffness of the structure. Many researchers (Pandey et al., 1991; Sampaio et al., 1999; Qiao et al., 2007; Guan and Karbhari, 2008; Wang et al., 2021) proposed strain-related modal parameters for structural damage diagnosis. While Li et al. (2017) directly used the dynamic strains to calculate the strain response covariance as a damage index and demonstrated the feasibility of the proposed damage detection method with the new index through numerical studies on a frame structure and experimental studies on a circular steel arch.

In the early stages of structural damage occurrence, effective response signals tend to be submerged in measurement noise, which is an obstacle to the damage identification. Li et al. (2004) investigated a method using a multiple autocorrelation method to remove the influence of noise and detect the weak sinusoidal signal buried in strong noise. Tang and Xing (2007) and Wang et al. (2015) studied the quadratic correlation function of signals. The results showed that the quadratic correlation function method can effectively suppress the noise in the measured signals and highlight the effective signal components.

According to the research results on the correlation function in structural damage detection and the quadratic correlation function in signal processing, the present study proposes a structural damage detection procedure based on the quadratic correlation function of strains (QCoS). This procedure does not require any analytical structural model. Compared to modal parameters, QCoS is easily constructed from dynamic strains in the time domain without the need for excitation measurements. First, QCoS is derived theoretically and proved to be a function of the modal parameters (frequency, strain mode shape and damping) of a structure under impact loading. QCoS contains sufficient modal information of the structure, even the modal information limited by the sampling frequency. Furthermore, the damage detection procedure based on QCoS with pattern matching degree (PMD) and QCoS change rate (QR) is proposed to detect the damage in a structure subjected to an unknown impact load. Numerical studies on a two-dimensional simply supported beam illustrate the performance of the proposed damage detection procedure. QCoS is found to be more sensitive to local damage than the first few modal

frequencies of the structure. The effects of excitation position, reference point selection and damage level on QCoS are then investigated. In addition, the influence of the measurement noise on the accuracy of the identification results is analyzed. Finally, laboratory tests on simply supported beams verify the effectiveness and applicability of the proposed method.

2 THEORY

2.1 Quadratic correlation function of strain responses

The equation of motion for a viscous damped structure with N degrees of freedom (N-DOFs) is given as

$$M\ddot{x}_{\mathrm{G}}(t) + C\dot{x}_{\mathrm{G}}(t) + Kx_{\mathrm{G}}(t) = Lf(t)$$
(1)

where M, C, K are $N \times N$ mass, damping and stiffness matrices, respectively. $\ddot{x}_{\mathrm{G}}(t)$, $\dot{x}_{\mathrm{G}}(t)$, $x_{\mathrm{G}}(t)$ are $N \times 1$ acceleration, velocity and displacement vectors, respectively. L is the $N \times 1$ mapping vector, and $f(t)$ is the excitation. $Lf(t)$ represents that the excitation is applied to the corresponding DOFs of the structure. The existence of zero initial conditions for the excitation input at the DOFs is assumed in this study.

The strain in finite elements is first derived as a function of nodal displacement using finite element theory. On this basis, an expression for the strain response is obtained. Defined x_m as the displacement vector of a node of the mth element, one can obtain (Li and Lu, 2001)

$$x_m = Pa_m$$
(2)

P is the matrix of the displacement function, which is generally a polynomial function. a_m is the coefficient vector of a polynomial function. The coefficients are undetermined constants. To determine a_m uniquely, the number of undetermined constants should be equal to the number of DOFs of the element. When the position coordinate of each node is determined, the vector x_{em} consisting of the displacements of all nodes for the mth element is expressed as

$$x_{em} = A_m a_m, \; a_m = A_m^{-1} x_{em}$$
(3)

A_m is a numeric matrix. Substituting Equation (3) into Equation (2), x_m is rewritten as

$$x_m = PA_m^{-1} x_{em}$$
(4)

For the mth element, the strain vector ε_m is expressed as

$$\varepsilon_m = Dx_m = DPA_m^{-1} x_{em} = B_m x_{em}, \; \left(m = 1, 2, ..., n_{\mathrm{e}}\right)$$
(5)

where $B_m = DPA_m^{-1}$, D is the differential operator, n_{e} is the number of elements. Using the differential operator D, the strain of the mth element is calculated from the nodal displacement of the element.

$$\varepsilon = Bx$$
(6)

where the vectors x and ε are the nodal displacement vector and the strain vector of n_{e} elements, respectively. Considering the continuous displacement condition of each element at the connection node, Equation (6) is converted to the global coordinate. By coordinate transformation, x is written as

$$x = \beta x_{\mathrm{G}}$$

(7)

where β is the coordinate transformation matrix, x_{G} the nodal displacement vector in global coordinate. Equation (6) is expressed as

$$\varepsilon = B\beta x_{\mathrm{G}} = \tilde{B} x_{\mathrm{G}}$$

(8)

Substituting Equation (8) into Equation (1), we get

$$M_{\varepsilon} \ddot{\varepsilon}(t) + C_{\varepsilon} \dot{\varepsilon}(t) + K_{\varepsilon} \varepsilon(t) = \tilde{B}^{-\mathrm{T}} L f(t)$$

(9)

where $M_{\varepsilon} = \tilde{B}^{-\mathrm{T}} M \tilde{B}^{-1}$, $C_{\varepsilon} = \tilde{B}^{-\mathrm{T}} C \tilde{B}^{-1}$, $K_{\varepsilon} = \tilde{B}^{-\mathrm{T}} K \tilde{B}^{-1}$.

The strain response is expressed as

$$\varepsilon(t) = \boldsymbol{\Phi}^{\varepsilon} q(t)$$

(10)

$\boldsymbol{\Phi}^{\varepsilon}$ is the *N×N* strain mode-shape matrix, and $q(t)$ with the size of *N×1* is the generalized coordinate vector of strain mode. Substituting Equation (10) into Equation (9), we have

$$M_r \ddot{q}(t) + C_r \dot{q}(t) + K_r q(t) = \psi f(t)$$

(11)

where $M_r = \boldsymbol{\Phi}^{\varepsilon\mathrm{T}} M_{\varepsilon} \boldsymbol{\Phi}^{\varepsilon}$, $C_r = \boldsymbol{\Phi}^{\varepsilon\mathrm{T}} C_{\varepsilon} \boldsymbol{\Phi}^{\varepsilon}$, $K_r = \boldsymbol{\Phi}^{\varepsilon\mathrm{T}} K_{\varepsilon} \boldsymbol{\Phi}^{\varepsilon}$, $\psi = \boldsymbol{\Phi}^{\varepsilon\mathrm{T}} \tilde{B}^{-\mathrm{T}} L$.

The unit impulse response function of the *l*th DOF of a structure is expressed as

$$h_l^{\varepsilon}(t) = \sum_{i=1}^{N} \frac{\Phi_{li}^{\varepsilon} \psi_i}{\omega_{di}} e^{-\xi_i \omega_i t} \sin(\omega_{di} t)$$

(12)

where ω_i, ω_{di}, ξ_i are the *i*th undamped modal frequency, damped modal frequency and damping ratio respectively. Φ_{li}^{ε} is the *l*th element of *i*th strain mode shape, $\psi_i = \Phi_i^{\varepsilon\mathrm{T}} \tilde{B}^{-\mathrm{T}} L$.

The strain response of the *l*th DOF of the structure under excitation $f(t)$ is written as (Clough and Penzien, 2003)

$$\varepsilon_l(t) = \int_{-\infty}^{t} f(\tau) h_l^{\varepsilon}(t-\tau) d\tau$$

(13)

When $\tau > t$, $h_l^{\varepsilon}(t-\tau) = 0$, Equation (13) is rewritten as

$$\varepsilon_l(t) = \int_{-\infty}^{\infty} f(\tau) h_l^{\varepsilon}(t-\tau) d\tau$$

(14)

The simulated strain responses of the DOFs *p*, *l* correspond to the strain responses collected from the measuring points *p*, *l* of the structure in a vibration test. When the structure is subjected to a unit impulse, the cross-correlation function of the strain responses is given as

$$R_{pl}(\tau) = \int_{-\infty}^{\infty} h_p^{\varepsilon}(t) h_l^{\varepsilon}(t+\tau) dt \tag{15}$$

When $t < 0$, there is no strain response measured from the structure, i.e., $h_l^{\varepsilon} = 0$. Equation (15) is rewritten as,

$$R_{pl}(\tau) = \int_0^{\infty} h_p^{\varepsilon}(t) h_l^{\varepsilon}(t+\tau) dt \tag{16}$$

Substituting Equation (12) into Equation (16), we have

$$R_{pl}(\tau) = \sum_{j=1}^{N} \sum_{i=1}^{N} \Phi_{pi}^{\varepsilon} \Phi_{lj}^{\varepsilon} \frac{\psi_i \psi_j}{\omega_{di} \omega_{dj}} e^{-\xi_j \omega_j \tau} [A_{ij} \cos(\omega_{dj}\tau) + B_{ij} \sin(\omega_{dj}\tau)]$$

$$= \sum_{j=1}^{N} \frac{\Phi_{lj}^{\varepsilon} \psi_j}{\omega_{dj}} e^{-\xi_j \omega_j \tau} \sum_{i=1}^{N} \frac{\Phi_{pi}^{\varepsilon} \psi_i}{\omega_{di}} [A_{ij} \cos(\omega_{dj}\tau) + B_{ij} \sin(\omega_{dj}\tau)]$$

$$= \sum_{j=1}^{N} \frac{\Phi_{lj}^{\varepsilon} \psi_j}{\omega_{dj}} e^{-\xi_j \omega_j \tau} \left\{ \left(\sum_{i=1}^{N} \frac{\Phi_{pi}^{\varepsilon} \psi_i}{\omega_{di}} A_{ij} \right) \cos(\omega_{dj}\tau) + \left(\sum_{i=1}^{N} \frac{\Phi_{pi}^{\varepsilon} \psi_i}{\omega_{di}} B_{ij} \right) \sin(\omega_{dj}\tau) \right\}$$

$$= \sum_{j=1}^{N} \frac{\Phi_{lj}^{\varepsilon} \psi_j}{\omega_{dj}} e^{-\xi_j \omega_j \tau} \left\{ G_j \cos(\omega_{dj}\tau) + H_j \sin(\omega_{dj}\tau) \right\} \tag{17}$$

where,

$$G_j = \sum_{i=1}^{N} \frac{\Phi_{pi}^{\varepsilon} \psi_i}{\omega_{di}} A_{ij} \quad H_j = \sum_{i=1}^{N} \frac{\Phi_{pi}^{\varepsilon} \psi_i}{\omega_{di}} B_{ij}$$

$$A_{ij} = \frac{1}{2} \left[\frac{\xi_i \omega_i + \xi_j \omega_j}{(\xi_i \omega_i + \xi_j \omega_j)^2 + (\omega_{di} - \omega_{dj})^2} - \frac{\xi_i \omega_i + \xi_j \omega_j}{(\xi_i \omega_i + \xi_j \omega_j)^2 + (\omega_{di} + \omega_{dj})^2} \right]$$

$$B_{ij} = \frac{1}{2} \left[\frac{\omega_{di} + \omega_{dj}}{(\xi_i \omega_i + \xi_j \omega_j)^2 + (\omega_{di} + \omega_{dj})^2} + \frac{\omega_{di} - \omega_{dj}}{(\xi_i \omega_i + \xi_j \omega_j)^2 + (\omega_{di} - \omega_{dj})^2} \right]$$

Equation (16) is expressed as,

$$R_{pl}(\tau) = \sum_{j=1}^{N} \Phi_{lj}^{\varepsilon} u_j^{\varepsilon}(p,\tau) = \boldsymbol{\Phi}_l^{\varepsilon} \boldsymbol{u}^{\varepsilon}(p,\tau) \tag{18}$$

where,

$$u_j^{\varepsilon}(p,\tau) = \frac{\psi_j}{\omega_{dj}} e^{-\xi_j \omega_j \tau} \left\{ G_j \cos(\omega_{dj}\tau) + H_j \sin(\omega_{dj}\tau) \right\}$$

$$\boldsymbol{u}^{\varepsilon}(p,\tau) = [u_1(p,\tau), u_2(p,\tau), ..., u_N(p,\tau)]^{\mathrm{T}}$$

$$\boldsymbol{\Phi}_l^{\varepsilon} = [\Phi_{l1}^{\varepsilon}, \Phi_{l2}^{\varepsilon}, ..., \Phi_{lN}^{\varepsilon}]$$

The quadratic correlation function matrix of strain response **Q** is expressed as

$$\boldsymbol{Q} = \boldsymbol{R}_{pl} \cdot \boldsymbol{R}_{pl}^{\mathrm{T}} = \boldsymbol{\Phi}^{\varepsilon} \boldsymbol{u}^{\varepsilon}(p) \cdot (\boldsymbol{\Phi}^{\varepsilon} \boldsymbol{u}^{\varepsilon}(p))^{\mathrm{T}} = \boldsymbol{\Phi}^{\varepsilon} (\boldsymbol{u}^{\varepsilon}(p) \cdot \boldsymbol{u}^{\varepsilon}(p)^{\mathrm{T}}) \boldsymbol{\Phi}^{\varepsilon\mathrm{T}}$$

(19)

where,

$$\boldsymbol{R}_{pl}(\tau) = \begin{bmatrix} R_{pl_1}(t_1) & R_{pl_1}(t_2) & ... & R_{pl_1}(t_n) \\ R_{pl_2}(t_1) & R_{pl_2}(t_2) & ... & R_{pl_2}(t_n) \\ ... & ... & ... & ... \\ R_{pl_g}(t_1) & R_{pl_g}(t_2) & ... & R_{pl_g}(t_n) \end{bmatrix}, \quad \boldsymbol{u}^{\varepsilon}(p) = \begin{bmatrix} u_1^{\varepsilon}(p,t_1) & u_1^{\varepsilon}(p,t_2) & ... & u_1^{\varepsilon}(p,t_n) \\ u_2^{\varepsilon}(p,t_1) & u_2^{\varepsilon}(p,t_2) & ... & u_2^{\varepsilon}(p,t_n) \\ ... & ... & ... & ... \\ u_N^{\varepsilon}(p,t_1) & u_N^{\varepsilon}(p,t_2) & ... & u_N^{\varepsilon}(p,t_n) \end{bmatrix}$$

$l_1 \sim l_g$ are g measuring points, and one of the points is used as the reference point p. When $p=l$, R_{pl} is the autocorrelation function of the strain response. $t_n = n\Delta t$, Δt is the time interval.

$$\left[\boldsymbol{u}^{\varepsilon}(p) \cdot \boldsymbol{u}^{\varepsilon}(p)^{\mathrm{T}}\right]_{i \times j} = \sum_n \boldsymbol{u}_i^{\varepsilon}(p,t_n) \boldsymbol{u}_j^{\varepsilon}(p,t_n)$$

$$= \sum_n \frac{\psi_i}{\omega_{di}} e^{-\xi_i \omega_i (n\Delta t)} \left\{ G_i \cos(\omega_{di}(n\Delta t)) + H_i \sin(\omega_{di}(n\Delta t)) \right\} \frac{\psi_j}{\omega_{dj}} e^{-\xi_j \omega_j (n\Delta t)} \left\{ G_j \cos(\omega_{dj}(n\Delta t)) + H_j \sin(\omega_{dj}(n\Delta t)) \right\}$$

$$= \frac{\psi_i \psi_j}{\omega_{di} \omega_{dj} \Delta t} \left\{ \sum_n e^{-(\xi_i \omega_i + \xi_j \omega_j)(n\Delta t)} G_i G_j \cos(\omega_{di}(n\Delta t)) \cos(\omega_{dj}(n\Delta t)) \Delta t \right.$$

$$+ \sum_n e^{-(\xi_i \omega_i + \xi_j \omega_j)(n\Delta t)} G_i H_j \cos(\omega_{di}(n\Delta t)) \sin(\omega_{dj}(n\Delta t)) \Delta t$$

$$+ \sum_n e^{-(\xi_i \omega_i + \xi_j \omega_j)(n\Delta t)} H_i G_j \sin(\omega_{di}(n\Delta t)) \cos(\omega_{dj}(n\Delta t)) \Delta t$$

$$+ \left. \sum_n e^{-(\xi_i \omega_i + \xi_j \omega_j)(n\Delta t)} H_i H_j \sin(\omega_{di}(n\Delta t)) \sin(\omega_{dj}(n\Delta t)) \Delta t \right\}$$

(20)

where the element at the ith row and jth column of the matrix $\left[\boldsymbol{u}^{\varepsilon}(p) \cdot \boldsymbol{u}^{\varepsilon}(p)^{\mathrm{T}}\right]$ is denoted as the subscript $i \times j$, and the subscript i and j denote the mode number of the structure. If n is large enough, i.e., the measuring time is long enough, the above equation can be expressed as,

$$\left[\boldsymbol{u}^{\varepsilon}(p)\cdot\boldsymbol{u}^{\varepsilon}(p)^{\mathrm{T}}\right]_{i\times j} = \frac{\psi_i\psi_j}{\omega_{di}\omega_{dj}\Delta t}\left\{G_iG_j\int_0^{+\infty}e^{-(\xi_i\omega_i+\xi_j\omega_j)t}\cos(\omega_{di}t)\cos(\omega_{dj}t)dt\right.$$

$$+G_iH_j\int_0^{+\infty}e^{-(\xi_i\omega_i+\xi_j\omega_j)t}\cos(\omega_{di}t)\sin(\omega_{dj}t)dt$$

$$+H_iG_j\int_0^{+\infty}e^{-(\xi_i\omega_i+\xi_j\omega_j)t}\sin(\omega_{di}t)\cos(\omega_{dj}t)dt$$

$$+H_iH_j\int_0^{+\infty}e^{-(\xi_i\omega_i+\xi_j\omega_j)t}\sin(\omega_{di}t)\sin(\omega_{dj}t)dt$$

(21)

Equation (21) is rewritten as,

$$\left[\boldsymbol{u}^{\varepsilon}(p)\cdot\boldsymbol{u}^{\varepsilon}(p)^{\mathrm{T}}\right]_{i\times j} = \frac{\psi_i\psi_j}{\omega_{di}\omega_{dj}\Delta t}\left\{\frac{G_iG_j}{2}\left[\frac{\xi_i\omega_i+\xi_j\omega_j}{\left(\xi_i\omega_i+\xi_j\omega_j\right)^2+\left(\omega_{di}+\omega_{dj}\right)^2}+\frac{\xi_i\omega_i+\xi_j\omega_j}{\left(\xi_i\omega_i+\xi_j\omega_j\right)^2+\left(\omega_{di}-\omega_{dj}\right)^2}\right]\right.$$

$$+\frac{G_iH_j}{2}\left[\frac{\omega_{di}+\omega_{dj}}{\left(\xi_i\omega_i+\xi_j\omega_j\right)^2+\left(\omega_{di}+\omega_{dj}\right)^2}-\frac{\omega_{di}-\omega_{dj}}{\left(\xi_i\omega_i+\xi_j\omega_j\right)^2+\left(\omega_{di}-\omega_{dj}\right)^2}\right]$$

$$+\frac{H_iG_j}{2}\left[\frac{\omega_{di}+\omega_{dj}}{\left(\xi_i\omega_i+\xi_j\omega_j\right)^2+\left(\omega_{di}+\omega_{dj}\right)^2}+\frac{\omega_{di}-\omega_{dj}}{\left(\xi_i\omega_i+\xi_j\omega_j\right)^2+\left(\omega_{di}-\omega_{dj}\right)^2}\right]$$

$$\left.-\frac{H_iH_j}{2}\left[\frac{\xi_i\omega_i+\xi_j\omega_j}{\left(\xi_i\omega_i+\xi_j\omega_j\right)^2+\left(\omega_{di}+\omega_{dj}\right)^2}-\frac{\xi_i\omega_i+\xi_j\omega_j}{\left(\xi_i\omega_i+\xi_j\omega_j\right)^2+\left(\omega_{di}-\omega_{dj}\right)^2}\right]\right\}$$

(22)

Equation (22) shows that the elements of matrix **Q** are functions of natural frequency, mode shape and damping ratio. The structural damage will lead to the change of elements of matrix **Q**. The elements of matrix **Q** can be adopted as the characteristic parameters for damage detection.

In structural vibration tests, measured strain responses are discrete signals. R_{pl} is computed as,

$$R_{pl}(\tau) = \frac{1}{n_s}\sum_{k=0}^{n_s-1}h_p^{\varepsilon}(k)h_l^{\varepsilon}(k+\tau)$$

(23)

where, n_s is the total number of collected signals, and τ is the time delay. Substituting Equation (23) into Equation (19), matrix **Q** is constructed as

$$Q = \begin{bmatrix} R_{pl_1}(t_1) & R_{pl_1}(t_2) & ... & R_{pl_1}(t_n) \\ R_{pl_2}(t_1) & R_{pl_2}(t_2) & ... & R_{pl_2}(t_n) \\ ... & ... & ... & ... \\ R_{pl_g}(t_1) & R_{pl_g}(t_2) & ... & R_{pl_g}(t_n) \end{bmatrix} \cdot \begin{bmatrix} R_{pl_1}(t_1) & R_{pl_1}(t_2) & ... & R_{pl_1}(t_n) \\ R_{pl_2}(t_1) & R_{pl_2}(t_2) & ... & R_{pl_2}(t_n) \\ ... & ... & ... & ... \\ R_{pl_g}(t_1) & R_{pl_g}(t_2) & ... & R_{pl_g}(t_n) \end{bmatrix}^{\mathrm{T}} = \begin{bmatrix} Q_{11} & Q_{12} & \cdots & Q_{1c} & Q_{1g} \\ Q_{21} & Q_{22} & \cdots & Q_{2c} & Q_{2g} \\ \vdots & \vdots & \vdots & \vdots & \vdots \\ Q_{r1} & Q_{r2} & \cdots & Q_{rc} & Q_{rg} \\ Q_{g1} & Q_{g2} & \cdots & Q_{gc} & Q_{gg} \end{bmatrix}$$

(24)

where, the element QCoS at the rth row and cth column of the matrix $\boldsymbol{Q}$ is denoted as Q_{rc}. Q_{rc} is computed by Equation (25). The subscripts r and c of Q_{rc} also correspond to the rth and cth measuring points (l_r and l_c) of the real structure, respectively.

$$Q_{rc} = \left[\boldsymbol{R}_{pl} \cdot \boldsymbol{R}_{pl}^{\mathrm{T}} \right]_{r \times c} = \sum_n R_{pl_r}(t_n) R_{pl_c}(t_n) \quad , \left(r, c = 1, 2, ..., g \right)$$

(25)

2.2 Pattern matching degree and QCoS change rate

Note that $\boldsymbol{Q}$ is symmetric according to Equation (24). The lower (or upper) triangular or diagonal elements are used to construct the damage feature vector V, as shown in Equation (26). After normalizing the vector V by Equation (27) to reduce the influence of different excitation amplitudes on Q_{rc}, the ratio between the components of the vector V remain constant, which is similar to the mode shape.

$$V = [Q_{11}, Q_{21}, Q_{22}, \cdots, Q_{r1}, Q_{r2}, \cdots, Q_{rr}, Q_{g1}, Q_{g2}, \cdots, Q_{gg}] \text{ or } = [Q_{11}, Q_{22}, \cdots, Q_{rr}, \cdots, Q_{gg}]$$

(26)

$$V_i = \frac{V_i}{\left\{ \sum_{i=1}^{n_c} V_i^2 \right\}^{1/2}} \quad , \left(i = 1 : n_c \right)$$

(27)

where the subscript i denotes the ith component of the damage feature vector, n_c is the total number of the vector components.

The damage feature vector of the structure in the undamaged or healthy state is defined as the baseline vector, and it is denoted by V^{r}. The difference between V of the structure in the unknown state and V^{r} is computed for structural damage identification. Allemang (2003) proposed the modal assurance criteria (MAC) expressed as Equation (28). It was used to calculate the correlation between the theoretical and measured mode shapes. MAC has been widely used as an indicator to evaluate the change of structural parameters in structural health monitoring (SHM). However, this indicator, generated by least squares-based linear regression analysis, is sensitive to the large differences rather than small changes between two sets of values (Allemang, 2003).

$$\mathrm{MAC} = \frac{\left[\sum_{i=1}^{n_c} \left(V_i \times V_i^{\mathrm{r}} \right) \right]^2}{\sum_{i=1}^{n_c} \left[V_i \right]^2 \times \sum_{i=1}^{n_c} \left[V_i^{\mathrm{r}} \right]^2} \quad , \left(i = 1 : n_c \right)$$

(28)

The pattern matching degree (PMD) is used in this paper to compare damage feature vectors before and after structural damage. The value of PMD is calculated by Equation (29).

$$P_i = \min\left(\frac{V_i}{V_i^{\mathrm{r}}}, \frac{V_i^{\mathrm{r}}}{V_i}\right), \left(i = 1 : n_{\mathrm{c}}\right)$$

$$\mathrm{PMD} = \frac{\sum\limits_{i=1}^{n_{\mathrm{c}}} P_i}{n_{\mathrm{c}}}$$

(29)

When V is identical to V^{r}, the values of both MAC and PMD are 1. If the structure is abnormal or damaged, the value is less than 1. It should be noted that the dynamic strain collected in the real bridge test for a long time contains the temperature effect component, such as strain generated by temperature stress, temperature drift, etc. This component cannot reflect the dynamic characteristics of the structure. If it is not eliminated, the strain auto/cross correlation function will change greatly, resulting in a misjudgment of the actual health status of the structure (Li et al., 2018). For the dynamic strain measured in a short time, this non-dynamic component in strain data mainly generated by temperature drift can be eliminated by detrending.

The QCoS change rate (QR$_i$) computed by Equation (30) represents the relative changes of each component of the damage feature vector V before and after structural damage, which can be used to locate the damage of a structure.

$$\mathrm{QR}_i = \frac{\partial V_i}{V_i^{\mathrm{r}}} = \frac{V_i - V_i^{\mathrm{r}}}{V_i^{\mathrm{r}}}, \left(i = 1 : n_{\mathrm{c}}\right)$$

(30)

3 NUMERICAL SIMULATION

A simply supported steel beam, as shown in Figure 1, is used for the numerical study. The physical properties of the material are the density ρ=7850kg/m³, Young's modulus E=206GPa and damping ratio ξ=0.025. The cross-section of the beam is 60mm (width) × 30mm (thickness) and the distance between two bearings is 2.7m. Due to the high span-depth ratio of the simulated beam, transversal shear effects are ignored in the calculation. Based on the Bernoulli-Euler beam theory, the finite element (FE) model of the simply supported beam is implemented by MATLAB software. The FE model consists of 9 2D beam elements with a total of 10 nodes and 3 degrees of freedom (DOFs) per node. Both ends of the simply supported beam rotate freely, with horizontal and vertical motions constrained at one end and only vertical motion constrained at the other end of the beam.

Measuring points l_1-l_8 of the strain responses are arranged along the upper surface of the beam. The distance between the measuring points and that between the bearing and the measuring point are both 30cm. The beam is subjected to a downward force in the form of a triangular impulse with a duration of 0.03s. Unless otherwise specified, the excitation with a peak value of 100N is applied to node 5 of the beam and l_2 is set as the reference point in the analysis of the numerical simulation. The vertical displacement responses of 8 measuring points are first calculated by the Wilson-θ algorithm and then the strain responses of the beam are further obtained. The sampling frequency is 1000Hz. A total of 5s of strain responses are calculated and 5000 data are got for each measuring point. White Gaussian noise is added to the strain samples to simulate the measurement noise, and the signal-to-noise ratio (SNR) is 80 dB.
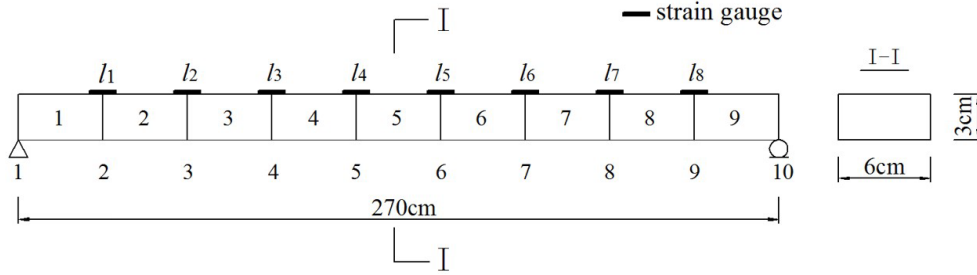
Figure 1 A simply supported beam model

3.1 Effect of excitation amplitude on QCoS

To analyze the effect of excitation amplitude on QCoS, the excitations with different peak values (100N and 200N) are respectively applied vertically to node 5 of the undamaged beam. The strain time histories of the beam show attenuation trends, such as the dynamic strains of measuring points 2 and 5 in Figure 2. The matrices Qs for two excitation cases are computed by Equation (23)~(24). Because there are 8 measuring points, the size of matrix Q is 8×8 with 36 independent elements. The damage feature vector V is formed by the lower triangular elements of matrix Q (Equation (26)) and normalized by Equation (27). As can be seen in Figure 3, the components of the normalized vectors Vs obtained from two excitation cases are identical. The MAC and PMD values calculated by Equation (28) and (29) are both greater than 0.99999. The small difference between two vectors may be caused by measurement noise. The results indicate that the ratios between components of V remain consistent after V is normalized to eliminate the effect of excitation amplitude on QCoS, and the normalized vector V of the undamaged beam can be used as the reference vector V^{r} for structural damage identification.
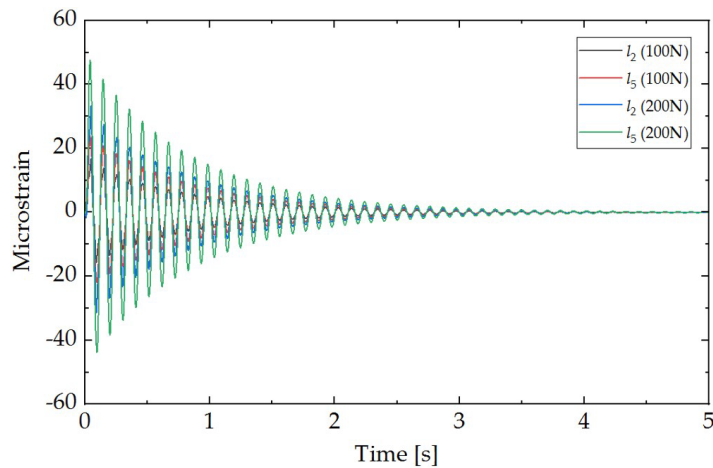

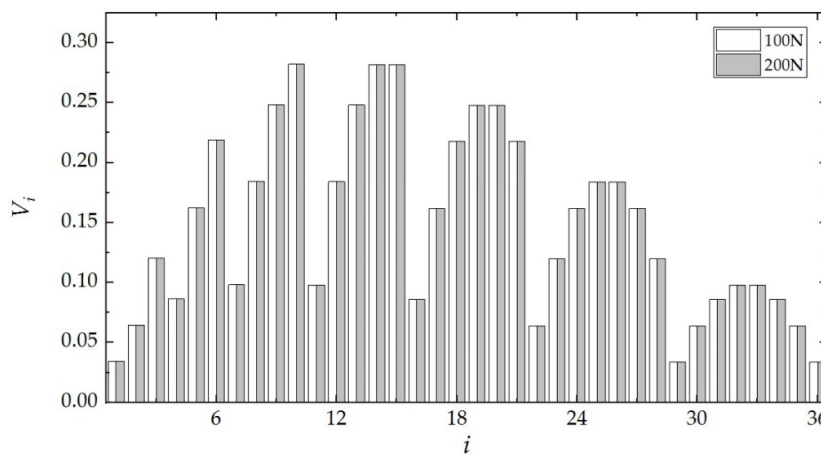**Figure 2** *Simulated responses of the measuring points l2 and l5 of the intact beam under different excitations*

Figure 3 Components of normalized damage feature vectors of the intact beam under different excitations

3.2 Effect of excitation position and reference point on QCoS

To further analyze the effect of the excitation position on QCoS, the impulse excitation with a peak value of 100N is applied vertically to nodes 2, 3, 4 and 5 of the undamaged beam respectively. The MAC and PMD values obtained by pairwise calculation of the normalized vectors *V*s in these four excitation position cases are greater than 0.99999. The components of the vectors *V*s are displayed in Figure 4. It can be seen that the components of the vector *V* do not vary as the excitation position on the beam changes.
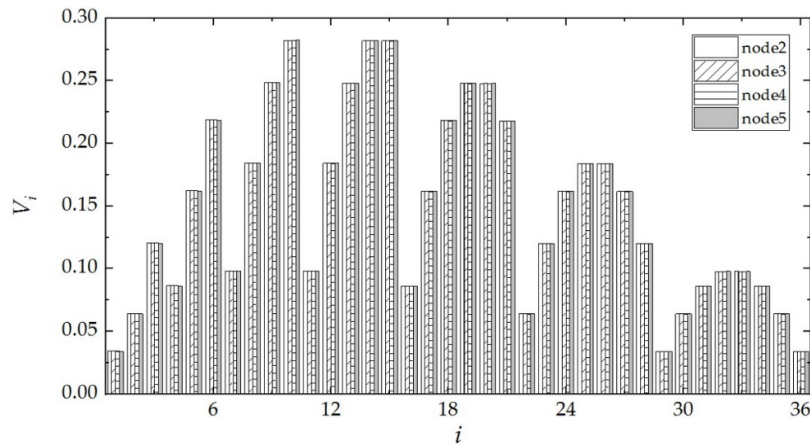

Figure 4 Components of normalized damage feature vectors of the intact beam obtained with excitations at different positions

Note that QCoS is calculated based on R_{pl} according to Equation (25). Here it is analyzed whether the different choices of the reference point p will cause the component in the normalized vector V to change. The strain sample analyzed is also obtained by applying an impulse excitation with a peak value of 100N to node 5 of the undamaged beam. In the four reference point cases, the measuring points l_1, l_2, l_3 and l_4 are set as the reference point p respectively, and the MAC and PMD values obtained by pairwise calculation of the normalized vectors Vs in four cases are also greater than 0.99999. The results show that the variation of the reference point in the calculation of QCoS does not lead to the changes in the components of the normalized damage feature vector V.

3.3 Effect of damage on QCoS

The damage is simulated by reducing the stiffness of the beam element, $\Delta k_m = -\Delta\alpha_m k_m$. $\Delta\alpha_m$ is a fractional change in the stiffness k of the mth element, $\Delta\alpha_m \in [0,1]$, (m=1, 2, …, 9). Three damage cases are described below.

case I:

(1) $\Delta\alpha_3 = 5\%$; (2) $\Delta\alpha_3 = 10\%$; (3) $\Delta\alpha_3 = 20\%$; (4) $\Delta\alpha_3 = 40\%$

case II:

(1) $\Delta\alpha_1 = 5\%$; (2) $\Delta\alpha_1 = 10\%$; (3) $\Delta\alpha_1 = 20\%$; (4) $\Delta\alpha_1 = 40\%$

case III:

(1) $\Delta\alpha_4 = 5\%$, $\Delta\alpha_1 = 10\%$; (2) $\Delta\alpha_4 = 10\%$, $\Delta\alpha_1 = 15\%$;

(3) $\Delta\alpha_4 = 20\%$, $\Delta\alpha_1 = 25\%$; (4) $\Delta\alpha_4 = 40\%$, $\Delta\alpha_1 = 45\%$

3.3.1 Sensitivity analysis

The relative sensitivity is obtained using Equations (31) and (32) respectively. The sensitivity of QCoS and modal frequency to local beam damage is compared.

$$\frac{\partial Q_{rc} / \partial\alpha}{Q_{rc}^{u}} = \frac{\left(Q_{rc}^{d} - Q_{rc}^{u}\right)/\partial\alpha}{Q_{rc}^{u}}$$

(31)

$$\frac{\partial f_i / \partial \alpha}{f_i^{\mathrm{u}}} = \frac{\left(f_i^{\mathrm{d}} - f_i^{\mathrm{u}}\right)/\partial \alpha}{f_i^{\mathrm{u}}}$$

(32)

where, the superscripts u and d denote the undamaged and damaged states of the structure respectively. f_i is the ith modal frequency.

The first 5 modal frequencies of the non-destructive beam are 9.56 Hz, 38.24 Hz, 86.10 Hz, 153.33Hz and 240.39Hz. For damage cases I(1) and case II(1), the relative sensitivities of the first 5 modal frequencies are listed in Tables 1 and 2, and the first 10 maximum values of the sensitivities of Q_{rc} are listed in Tables 3 and 4. The maximum absolute value of the relative sensitivity of frequency is only 0.1077, which is significantly less than that of QCoS, as shown in Figure 5. This analysis indicates that QCoS is more sensitive to structural damage than modal frequency. The stiffness-reduced element 3 is located between measuring points l_2 and l_3, the sensitivity values of Q_{22}, Q_{32}, Q_{33} in damage case I(1) are greater than other values of Q_{rc} in Table 3. The stiffness reduced element 1 is arranged with only one measuring point l_1, the sensitivity value of Q_{11} in damage case II(1) is significantly greater than the other values of Q_{rc} in Table 4. The results show that the change in Q_{rc} calculated from the strain responses measured by strain gauges placed at the node of the stiffness-reduced beam element is more pronounced.

Table 1 Relative sensitivity of f_i for damage case I(1)

f_i	f_1	f_2	f_3	f_4	f_5
Relative sensitivity	-0.0682	-0.1077	-0.0339	-0.0274	-0.0815

Table 2 Relative sensitivity of f_i for damage case II(1)

f_i	f_1	f_2	f_3	f_4	f_5
Relative sensitivity	-0.0046	-0.0173	-0.0344	-0.0509	-0.0632

Table 3 Relative sensitivity of Q_{rc} for damage case I(1)

Q_{rc}	Q_{22}	Q_{32}	Q_{33}	Q_{52}	Q_{62}	Q_{72}	Q_{82}	Q_{53}	Q_{63}	Q_{42}
Relative sensitivity	0.9869	0.9366	0.8875	0.3540	0.3399	0.3366	0.3330	0.3077	0.2916	0.2906

Table 4 Relative sensitivity of Q_{rc} for damage case II(1)

Q_{rc}	Q_{11}	Q_{31}	Q_{41}	Q_{51}	Q_{61}	Q_{71}	Q_{81}	Q_{21}	Q_{33}	Q_{43}
Relative sensitivity	1.0091	0.4934	0.4898	0.4884	0.4879	0.4879	0.4874	0.4562	-0.100	-0.0145

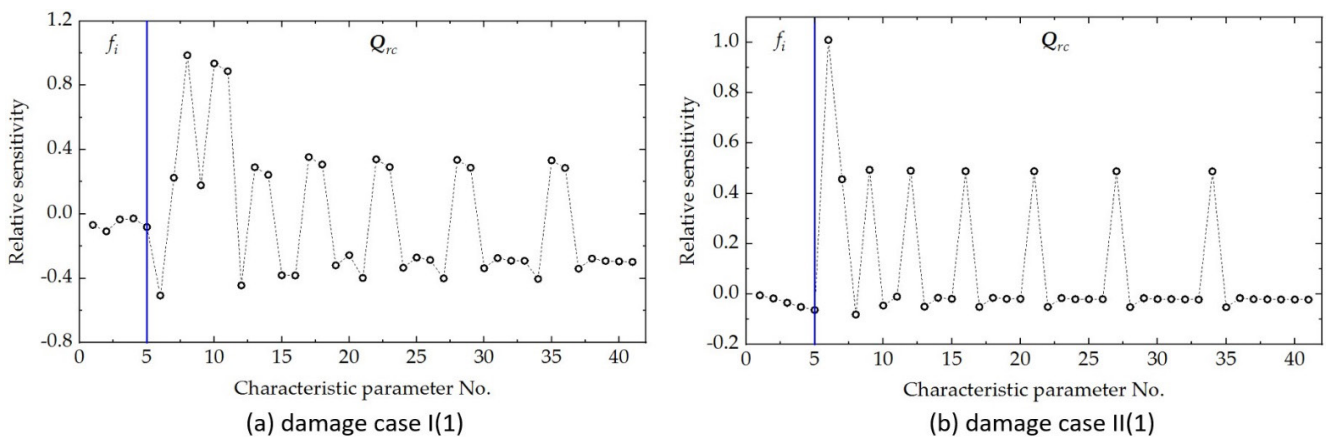
(a) damage case I(1)   (b) damage case II(1)

Figure 5 Comparison of the relative sensitivity of QCoS and frequency

3.3.2 Damage level

For damage case I, the stiffness of element 3 is reduced from 5 % to 40 %. As shown in Figure 6, the dotted lines indicate that Q_{rc} gradually increases as the element stiffness decreases. Q_{22}, Q_{32} and Q_{33}, calculated from the responses collected at measuring point l_2 or l_3 (located at nodes 3 and 4 of element 3), i.e., r and c=2 or 3, increase significantly. When r or c=2 or 3, the following Q_{rc} increase slightly: Q_{21}, Q_{31}, Q_{42}, Q_{43}, Q_{52}, Q_{53}, Q_{62}, Q_{63}, Q_{72}, Q_{73}, Q_{82} and Q_{83}. When r and c≠2 or 3, Q_{rc} decreases as the stiffness of element 3 decreases, such as Q_{11}, Q_{41}, Q_{44}, Q_{54}, etc.

Since Q_{22} and Q_{33} increase significantly in damage case I, the diagonal elements of the matrix **Q** are selected for analysis in damage case II. As shown in Figure 7, only Q_{11} increases with the stiffness reduction of element 1. In addition, the increase of Q_{11} in case II is less than that of Q_{22} and Q_{33} in case I. The same stiffness reduction of the different beam elements results in a different change in the value of Q_{rc}.

In damage case III, multiple damages are introduced to the beam, the stiffness of beam element 4 is reduced from 5 % to 40 % and that of element 1 is reduced from 10 % to 45 %. In the x coordinate of Figure 8, the value outside the parentheses represents the fractional reduction in the stiffness of element 4 and that inside the parentheses represents the fractional reduction in the stiffness of element 1. For example, in case III (1), the stiffness of element 4 is reduced by 5%, while the stiffness of element 1 is reduced by 10%. The increase of Q_{33}, Q_{43} and Q_{44} is greater than that of the following Q_{rc}: Q_{11}, Q_{31}, Q_{41}, Q_{61}, Q_{63}, Q_{64}, Q_{71}, Q_{73}, Q_{74}, Q_{81}, Q_{83} and Q_{84}. When r and c = 1 or 3 or 4, Q_{rc} increases as the stiffness of elements 1 and 4 decreases. When r or c=1 or 3 or 4, the stiffness reduction of the beam elements results in an increase of Q_{61}, Q_{63}, Q_{74}, etc. and a decrease of Q_{21}, Q_{32}, Q_{42}, etc. The results show that Q_{rc} is not certain to increase if only one of the measuring points (l_r or l_c) is located at the node of the stiffness-reduced element. Therefore, the stiffness-reduced beam elements cannot be accurately specified by the increase in the value of the off-diagonal element Q_{rc}. When r and c≠1 or 3 or 4, Q_{rc} decreases with the stiffness reduction of the structural elements 1 and 4, such as Q_{22}, Q_{52}, Q_{76}, Q_{85}, Q_{87}.
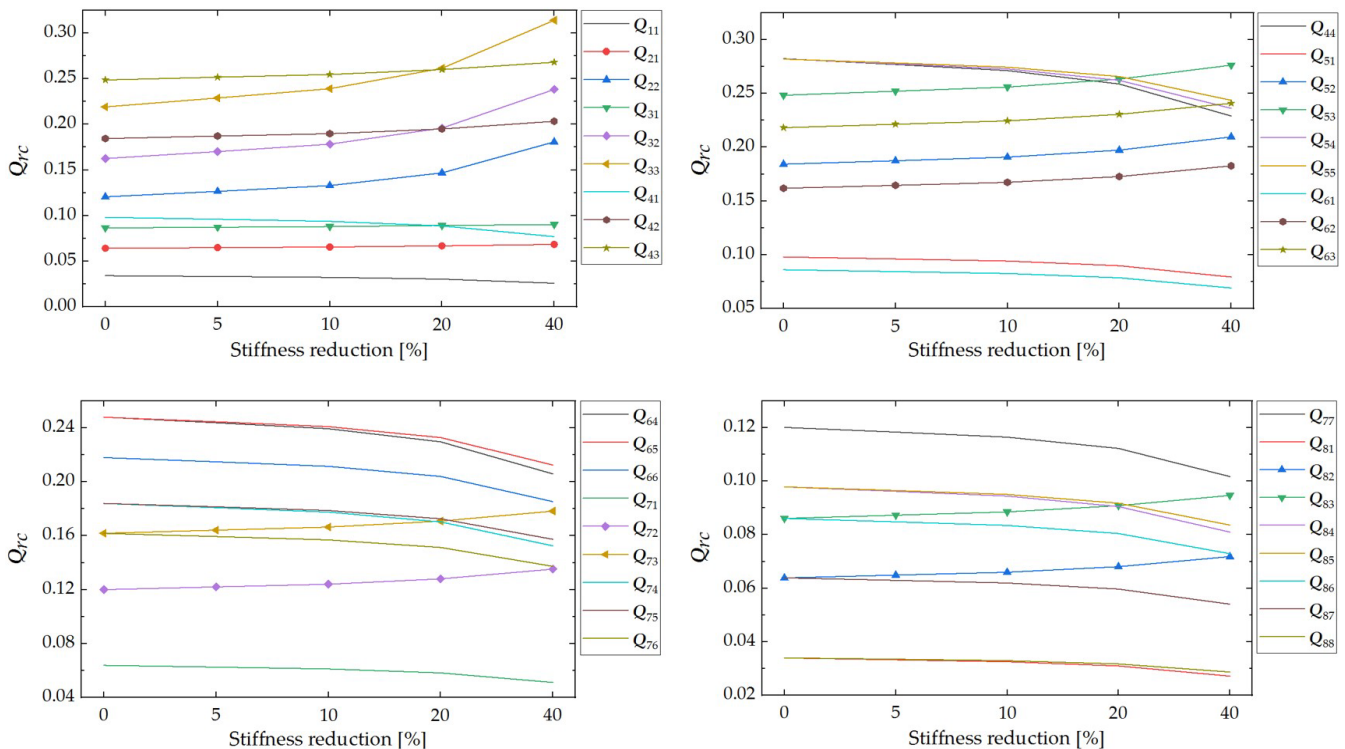

Figure 6 Curves of Q$_{rc}$ versus damage level (damage case I)
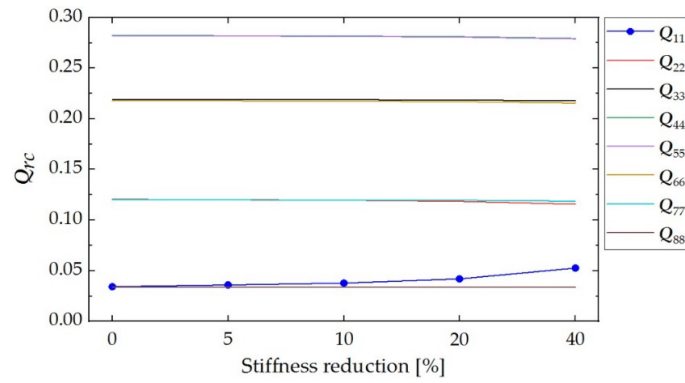
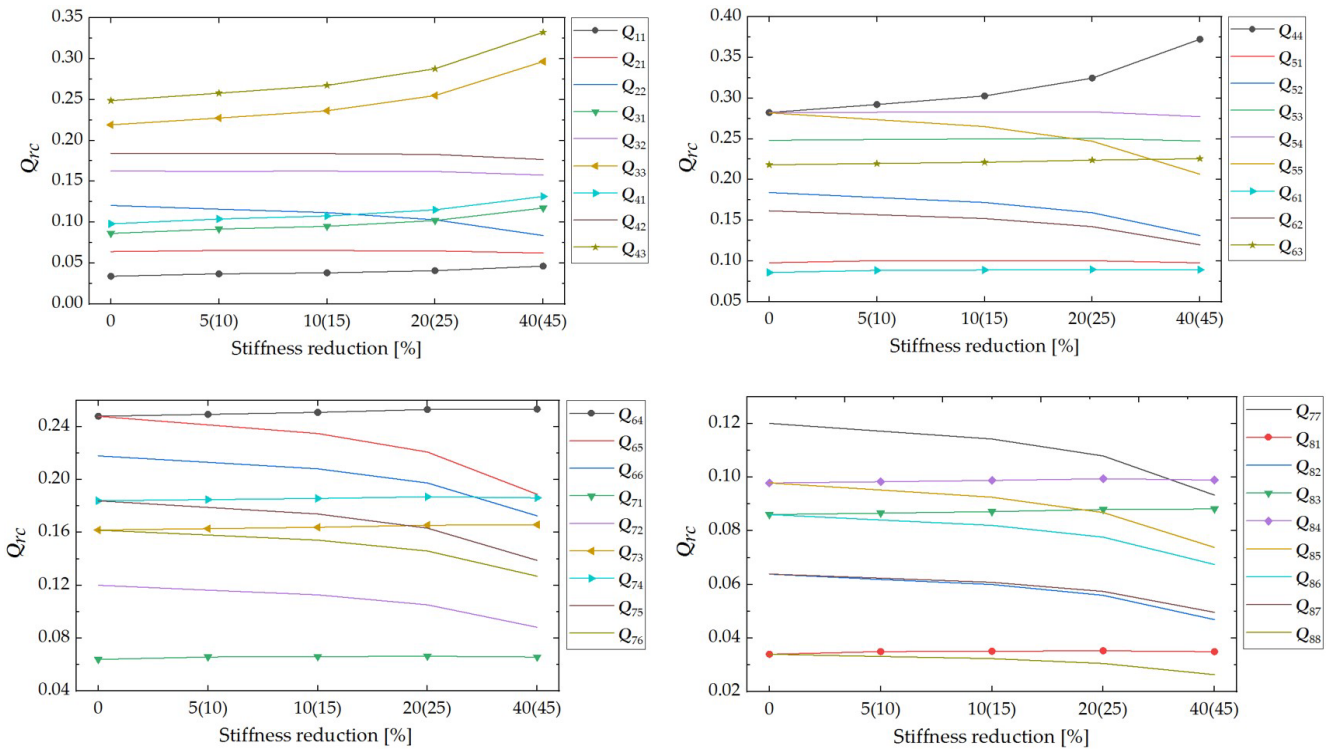**Figure 7** *Curves of Q$_{rc}$ versus damage level (damage case II)*

Figure 8 Curves of Q$_{rc}$ versus damage level (damage case III)

3.4 Damage detection

3.4.1 Damage detection procedure

By analyzing the variation of QCoS due to structural damage, it is found that the diagonal elements with increasing values in the matrix ***Q*** can be used to specify the stiffness-reduced element of the beam. The diagonal elements of the matrix ***Q*** are more suitable than the off-diagonal elements to form the damage feature vector *V*. The structural damage identification steps in Figure 9 are as follows:

Step.1 The dynamic strains of the undamaged structure subjected to impulse excitation are measured and the auto/cross correlation function R_{pl} is calculated by Equation (23). R_{pl} is then substituted into Equation (24) to calculate the matrix ***Q***. The damage feature vector *V* is constructed from the diagonal elements of the matrix ***Q*** and normalized as the reference vector V^{r}.

Step.2 Repeat Step 1 to obtain the vector *V* of the structure in the unknown state.

Step.3 To judge whether the structure is abnormal, the value of the pattern matching degree between *V* and V^{r} is calculated using Equation (29).

Step.4 The QCoS change rate (QR$_i$) as damage index is computed by Equation (30).

Step.5 Determine and locate the damage to a structure by combining PMD and QCoS change rate values.
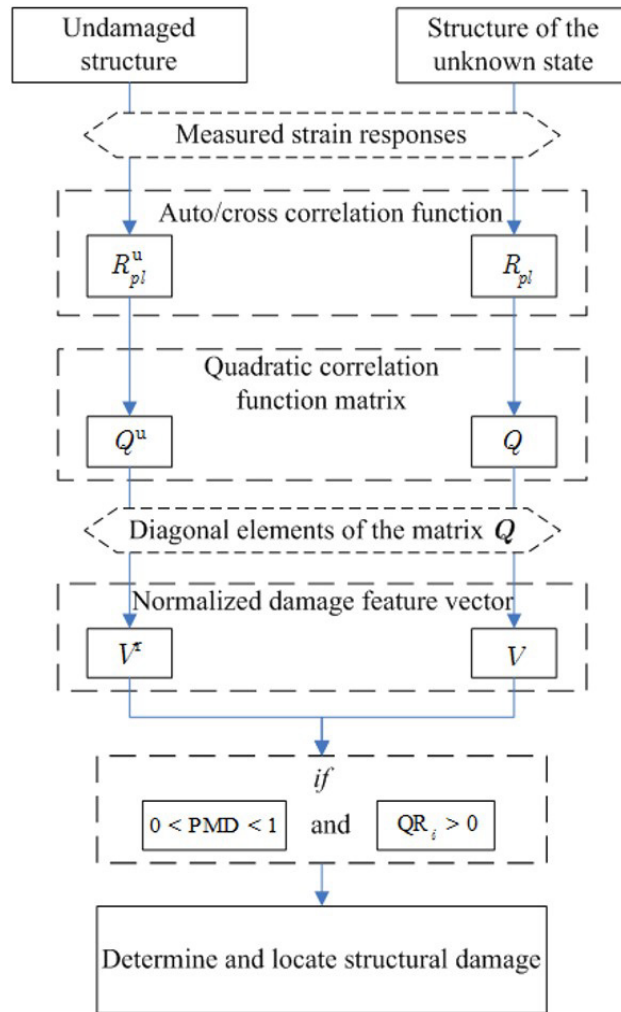
Figure 9 Damage detection procedure

3.4.2 Damage determination and localization

In general, the PMD and MAC values shown in Table 5 decrease as the severity of the structural damage increases. The MAC values are shown here for comparison. It can be seen that the PMD values decrease more significantly than the MAC values for the same level of structural damage. The 5% stiffness reduction of a single beam element in case I(1) and case II(1) causes the PMD value to decrease slightly to 0.9771 and 0.9933 respectively, while the MAC values are close to 1. The PMD values have reflected the change in vector V produced by the minor structural damage. When the stiffness of element 3 in case I(4) and element 1 in case II(4) both decrease by 40%, the PMD values drop to 0.79 and 0.9494 respectively. The same level of damage, occurring at the end and near the mid span of the beam respectively, has caused a different degree of change in the vector V.

According to the analyses of increased Q_{rc}, QR_i calculated by Equation (30) with a positive value can indicate the location of the structural damage. For case I, only QR_2 and QR_3 shown in Figure 10(a) are positive. The element with reduced stiffness is identified as being located beween two adjacent measuring points l_2 and l_3, i.e., element 3. For case II, only one measuring point l_1 is placed at node 2 of element 1, QR_1 is positive and QR_2 is negative, as shown in Figure 10(b). This indicates that the reduction in stiffness is likely to take place on the element 1. In case III, the values of QR_1 and QR_3 and QR_4 are positive as shown in Figure 10(c). Based on the results of the damage detection in case I and II, it can be judged that the stiffness reductions have occurred on elements 1 and 4.

Table 5 PMD and MAC values of damage cases

Damage case	I(1)	I(2)	I(3)	I(4)	II(1)	II(2)	II(3)	II(4)	III(1)	III(2)	III(3)	III(4)
PMD	0.9771	0.9535	0.9037	0.7900	0.9933	0.9868	0.9740	0.9494	0.9636	0.9333	0.8711	0.7416
MAC	0.9994	0.9972	0.9875	0.9370	0.9999	0.9999	0.9998	0.9987	0.9990	0.9958	0.9824	0.9244

(a) damage case I
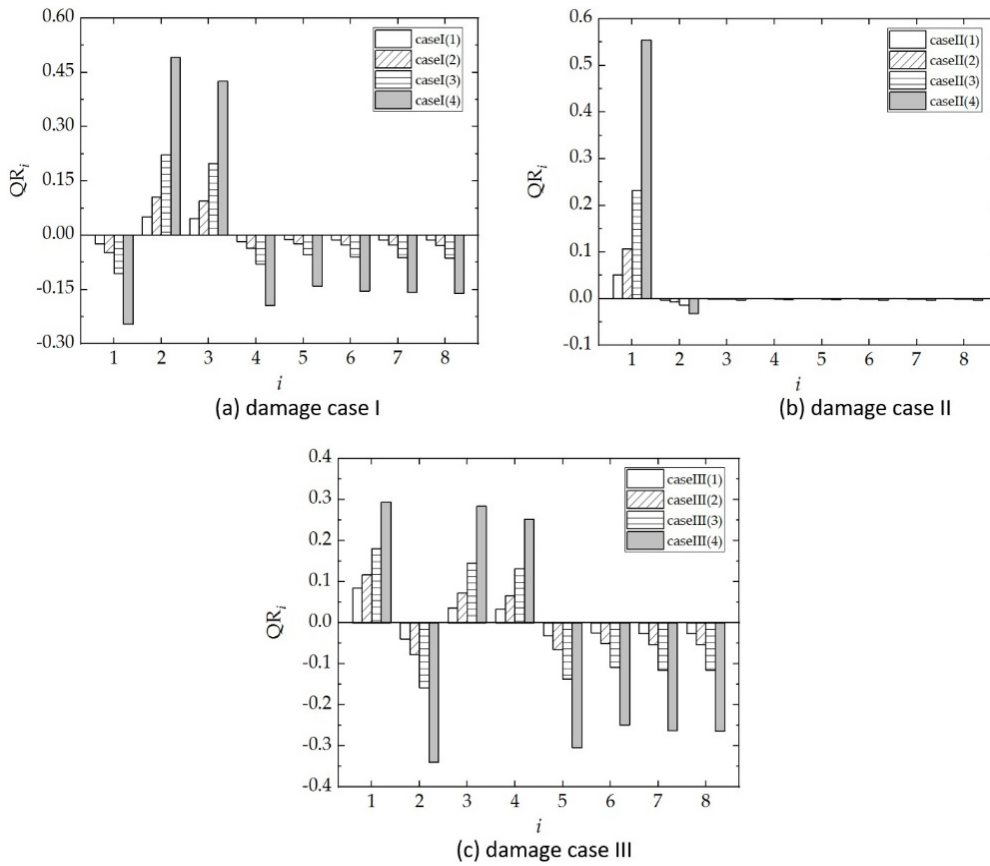
(b) damage case II

(c) damage case III

Figure 10 *Damage localization based on* QR_i

3.4.3 Effect of measurement noise on damage detection

The SNR of the strain responses analyzed previously is 80dB. In this section, the SNR of the responses in case I(1) and case III(1) are reduced to 60dB, 40dB and 20dB respectively to analyze whether the increase in noise level affects the accurate identification of small structural damage. The values of QR_i in Figure 11 are consistent for the structure in these two damage cases, and the structural damage can be correctly detected according to $QR_i>0$. When the SNR is 20 dB, the PMD value of case I(1) is 0.9764 and that of case III(1) is 0.9631. Comparing the values of case I(1) and case III(1) in Table 5, it can be seen that the PMD values hardly change when the SNR of the strain signals decreases from 80dB to 20dB. The results indicate that the components of the damage feature vector *V* are insensitive to the measurement noise, proving the point of view in the article (Tang and Xing, 2007) that the quadratic correlation method can greatly reduce the influence of noise on the signals.
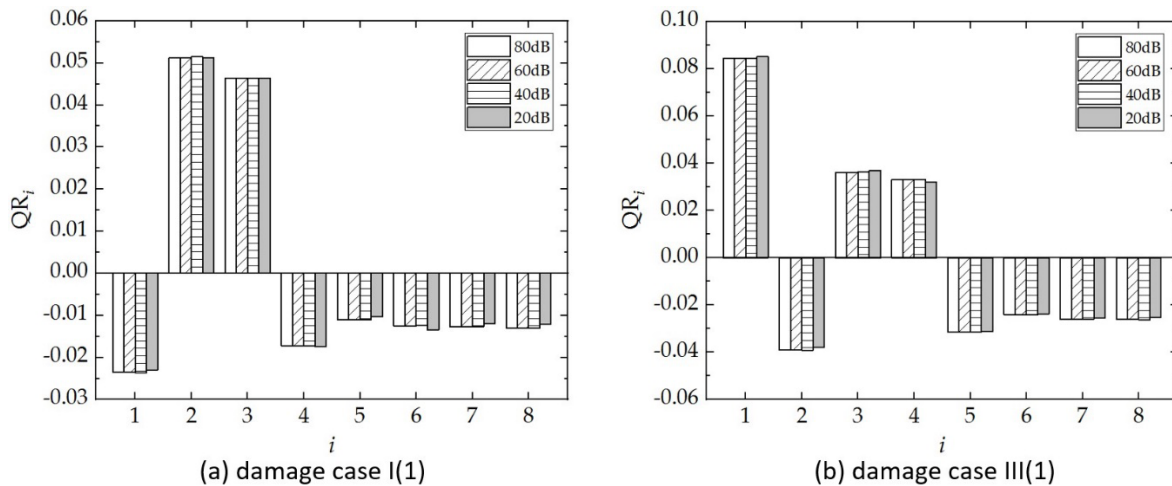

(a) damage case I(1)

(b) damage case III(1)

Figure 11 QR_i *at various noise levels*

4 EXPERIMENT VALIDATION

To investigate the performance of the proposed damage identification procedure with QCoS, three simply supported aluminum beams with the same span length and cross section are tested in the laboratory. All three beams have a cross section of 10cm (width) x 2cm (thickness) and a span of 270cm. One of the beams (beam 0), which is non-destructive, is used to develop the baseline for damage detection. The other two beams are cut on one side. Beam 1 is set with 1 cut and this cut, which is located at mid-span, is 20cm (length) x 3cm (width) x 2cm (thickness). Beam 2 is set with 2 cuts. One of the cuts, also at mid-span of the beam, is 20cm (length) x 4cm (width) x 2cm (thickness). The other cut is 20cm (length) x 2cm (width) x 2cm (thickness) and 5cm away from the adjacent bearing of beam 2. The cuts of beam 1 and beam 2 are marked with red rectangles in Figure 12(a).

8 strain gauges are mounted at equal intervals along the mid-line of the upper surface of all three beams in Figure 12(a). The distance between the measuring points and that between the center of the bearing and the measuring point are both 30cm. Impact excitation is applied downward with a steel hammer between measuring points 2 and 3 on the mid-line of the beam surface. The strain responses at 8 measuring points are collected by using the NI PXIe-1082 portable data acquisition system at a sampling frequency of 1000Hz. A total of 15s of strain responses are measured, and 15000 data are got for each measuring point. All detrended responses are shown in Figure 13.
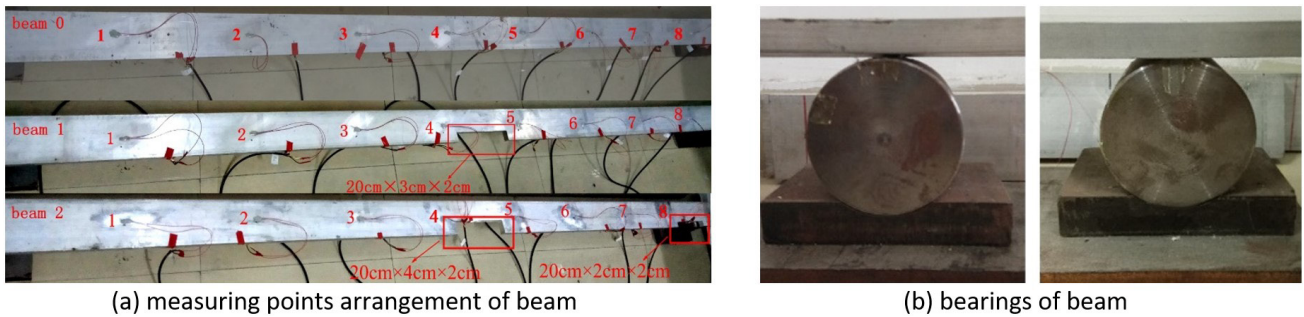

(a) measuring points arrangement of beam   (b) bearings of beam

Figure 12 Simply-supported beams in experiment

(a) NI PXIe-1082   (b) Strain responses of the beam 0

(c) Strain responses of the beam 1   (d) Strain responses of the beam 2
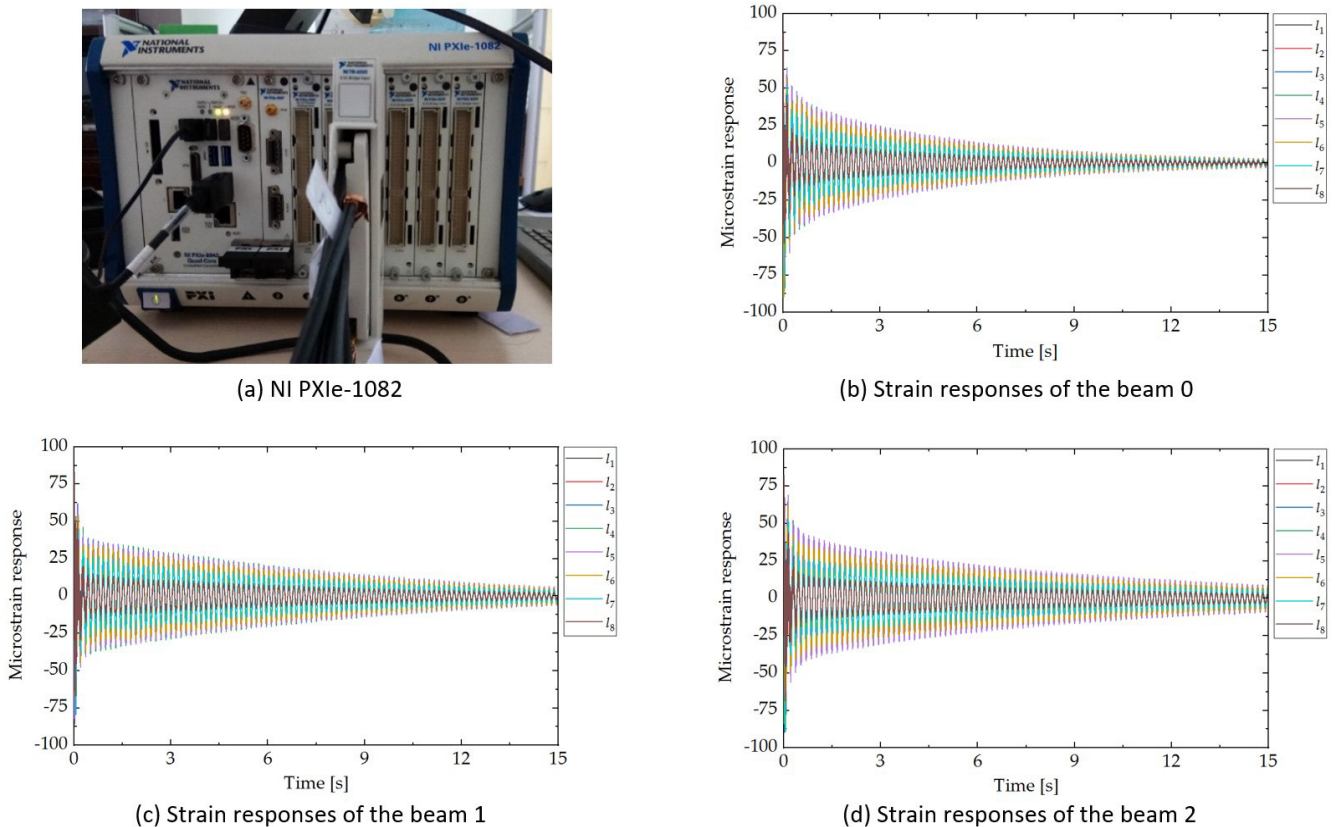
Figure 13 Data acquisition system and measured strain responses

According to the damage identification process, the auto/cross correlation functions are first calculated from Equation (23) using the strain data for each beam with measuring point 1 as the reference point (i.e., $p=1$). The matrix Q is then calculated using Equation (24) and the damage feature vector V is formed from the diagonal elements of the matrix Q. The components of the normalized damage feature vectors of 3 beams are shown in Figure 14. Using the vector of beam 0 as the reference vector V^r, the PMD values computed from Equation (29) for beam 1 and beam 2 are 0.8266 and 0.7341 respectively. As the size and number of cuts increase, the PMD value obviously decreases. It reflects the damage aggravation of the beam. As shown in Figure 15(a), QR_4 and QR_5 are positive, indicating that the damage is located in the segment of beam 1 between measuring points 4 and 5, i.e., the mid-span cut of the beam. Compared to Figure 15(a), QR_8 is positive in Figure 15(b). This suggests that there is one more damage at the end of beam 2 than beam 1.
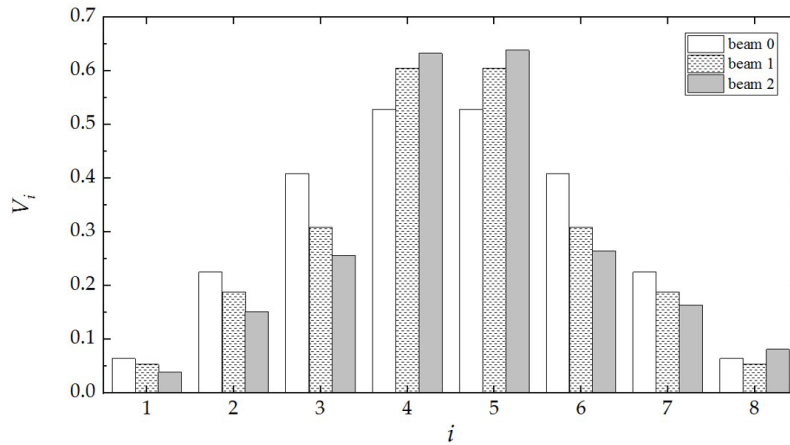

Figure 14 Components of damage feature vector of experimental beams
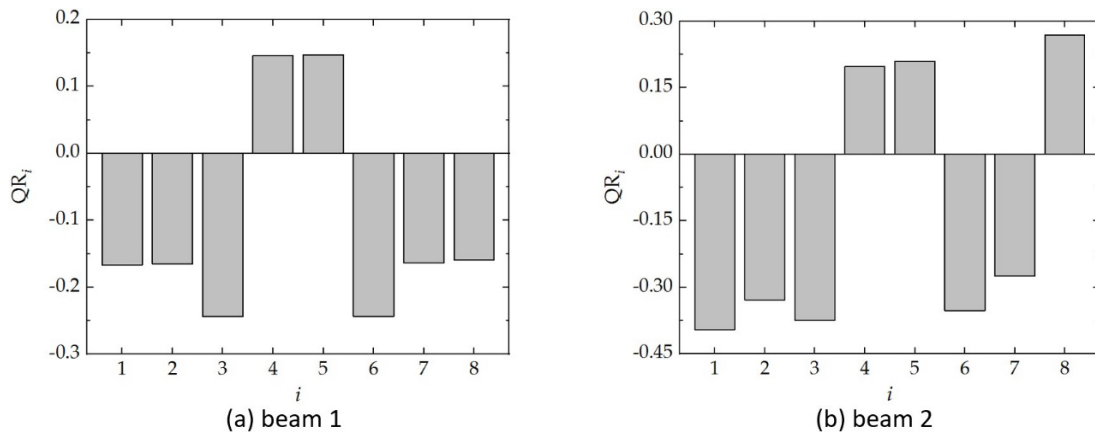

(a) beam 1   (b) beam 2

Figure 15 Damage localization for beam 1&2

5 CONCLUSION

A structural damage detection method based on the quadratic correlation function of strain responses (QCoS) is proposed. In vibration testing of a structure, QCoS is calculated in the time domain by strain responses. This damage detection method without the need of structural analytical model and modal parameter identification is convenient for engineering application. The QCoS of a structure under impact loading is proved to be a function of the modal frequency, mode shape and damping ratio. QCoS can be used to construct the damage feature vector, and if the structural state (intact or damaged) does not change, the ratio between the components of the normalized damage feature vector should remain constant. Therefore, it is theoretically possible to detect the damage using the difference between the normalized damage feature vectors (i.e., QCoS change rate) before and after the occurrence of damage to the structure. The PMD values are calculated to compare the normalized damage feature vectors of the unknown and intact states of the structure to preliminarily judge whether the structure is abnormal. The damage to the beam can then be definitively determined and located by the QCoS change rate (QR).

According to numerical studies on a simply supported steel beam with a high span-depth ratio, some conclusions are obtained as follows.

(1) The variations of the excitation position and the reference point for the structure do not lead to changes of the components (QCoSs) in the normalized damage feature vector. The normalized damage feature vector of the intact beam can be used as the baseline vector for structural damage identification.

(2) QCoS is more sensitive to local damage in the structure than frequency. Even a single slight damage to the beam produces the change of QCoS in the normalized damage feature vector.

(3) With the aggravation of the damage or the occurrence of multiple damages, the normalized damage feature vector of the destructive beam obviously differs from the baseline vector. It is reflected in the significant decrease of the PMD value and indicates that the structure is in an abnormal state.

(4) The QCoS in the normalized damage feature vector of the damaged beam, calculated from the responses collected at measuring point located at ends of the damaged beam segment, are greater than the corresponding QCoS in the baseline vector. The increase in the number of positive QR indicates that single damage develops into multiple damages on the simply supported beam. The ends of the damaged beam segment are located by the positive QR, and then the locations of multiple damages in the beam are accurately determined.

(5) When the SNR of the strain signals drops from 80 dB to 20dB, the PMD values of the minor damage cases show that the QCoSs in the normalized damage feature vector hardly change. QCoS has good robustness to measurement noise.

In an impact test on a structure, measured dynamic strains often contain the component generated by temperature drift, which does not reflect the dynamic properties of a structure and causes the non-damage induced change in the strain auto/cross correlation function. This component should be eliminated by detrending before calculating QCoS to avoid misjudging the structural state. Through the proposed damage identification method based on QCoS, the damages at the mid-span and the end of the simply supported aluminum beams in the laboratory experiments are accurately identified and located. It should be noted that the validity of the method is verified by numerical and laboratory tests based on the beam with a high span-depth ratio. For the short and deep beam, the shear effect needs to be considered and the effectiveness of this method requires further study.

Author's Contributions: Conceptualization, M Li; Methodology, M Li and TL Huang; Writing - original draft, M Li; Writing - review & editing, TL Huang; Funding acquisition, M Li and TL Huang.

Editor: Pablo Andrés Muñoz Rojas

References

Allemang, R. J. (2003). The modal assurance criterion-twenty years of use and abuse. Sound and Vibration 37(8): 14-23.

Clough, R.W. and Penzien, J. (2003). Dynamics of structures, Computers and Structures, Inc (the United States of America).

De Medeiros, R., Sartorato, M., Vandepitte, D., Tita, V. (2016). A comparative assessment of different frequency based damage detection in unidirectional composite plates using MFC sensors. Journal of Sound and Vibration 383: 171-190. DOI: 10.1016/j.jsv.2016.06.047.

De Medeiros, R., Vandepitte, D., Tita, V. (2018). Structural health monitoring for impact damaged composite: a new methodology based on a combination of techniques. Structural Health Monitoring 17:185-200. DOI: 10.1177/1475921716688442.

Deraemaeker, A., Reynders, E., De Roeck, G., Kullaa, J. (2008). Vibration-based structural health monitoring using output-only measurements under changing environment. Mechanical Systems and Signal Processing 22(1): 34-56. DOI: 10.1016/j.ymssp.2007.07.004.

Guan, H., Karbhari, V.M. (2008). Improved damage detection method based on element modal strain damage index using sparse measurement. Journal of Sound and Vibration 309(3-5): 465-494. DOI: 10.1016/j.jsv.2007.07.060.

Gul, M., Catbas, F.N. (2008). Ambient vibration data analysis for structural identification and global condition assessment. Journal of Engineering Mechanics 134(8): 650-662. DOI: 10.1061/(asce)0733-9399(2008)134:8(650).

He, W.Y., He, J., Ren, W.X. (2018). Damage localization of beam structures using mode shape extracted from moving vehicle response. Measurement 121: 276-285. DOI: 10.1016/j.measurement.2018.02.066.

Huth, O., Feltrin, G., Maeck, J., Kilic, N., Motavalli, M. (2005). Damage identification using modal data: Experiences on a prestressed concrete bridge. Journal of Structural Engineering 131(12): 1898-1910. DOI: 10.1061/(Asce)0733-9445(2005)131:12(1898).

Li, D.B. and Lu, H.Q. (2001). Experiment modal analysis and its application, Science Press (China).

Li, M., Ren, W.X., Huang, T.L., Wang, N.B. (2018). Experimental investigations on the cross-correlation function amplitude vector of the dynamic strain under varying environmental temperature for structural damage detection. Journal of Low Frequency Noise, Vibration and Active Control 39: 631-649. DOI: 10.1177/1461348418820237.

Li, X.Y., Law, S.S. (2010). Matrix of the covariance of covariance of acceleration responses for damage detection from ambient vibration measurements. Mechanical Systems and Signal Processing 24(4): 945-956. DOI: 10.1016/j.ymssp.2009.10.007.

Li, X.Y., Wang, L.X., Law, S.S., Nie, Z.H. (2017). Covariance of dynamic strain responses for structural damage detection. Mechanical Systems and Signal Processing 95: 90-105. DOI: 10.1016/j.ymssp.2017.03.020.

Li, Y.B., Yue, X., Yang, X.Y. (2004). Estimation of sinusoidal parameters in powerful noise by multi-layer autocorrelation. Journal of Harbin Engineering University 25: 525-528. (in Chinese).

Lou, J., Wu, L., Ma, L., Xiong, J., Wang, B. (2014). Effects of local damage on vibration characteristics of composite pyramidal truss core sandwich structure. Composites part B: Engineering: 62: 73-87. DOI: 10.1016/j.compositesb.2014.02.012.

Lu, L., Song, H., Huang, C. (2017). Effects of random damages on dynamic behavior of metallic sandwich panel with truss core. Composites Part B: Engineering 116: 278-290. DOI: 10.1016/j.compositesb.2016.10.051.

Manoach, E., Samborski, S., Mitura, A., Warminski, J. (2012). Vibration based damage detection in composite beams under temperature variations using Poincaré maps. International Journal of Mechanical Sciences, 62: 120-132. DOI: 10.1016/j.ijmecsci.2012.06.006.

Manoach, E., Warminski, J., Kloda, L., Teter, A. (2017). Numerical and experimental studies on vibration based methods for detection of damage in composite beams. Composite Structures, 170: 26-39. DOI: 10.1016/j.compstruct.2017.03.005

Medeiros, R.D., Souza, G.S.C., Marques, D.E.T., Flor, F.R., Tita, V. (2021). Vibration-based structural monitoring of bi-clamped metal-composite bonded joint: experimental and numerical analyses. The Journal of Adhesion 97: 891-917. DOI: 10.1080/00218464.2020.1711742

Nair, K.K., Kiremidjian, A.S., Law, K.H. (2006). Time series-based damage detection and localization algorithm with application to the ASCE benchmark structure. Journal of Sound and Vibration 291(1-2): 349-368. DOI: 10.1016/j.jsv.2005.06.016.

Omenzetter, P., Brownjohn, J.M.W., Moyo, P. (2004). Identification of unusual events in multi-channel bridge monitoring data. Mechanical Systems and Signal Processing 18(2): 409-430. DOI: 10.1016/s0888-3270(03)00040-2.

Pandey, A.K., Biswas, M., Samman, M.M. (1991). Damage detection from changes in curvature mode shapes. Journal of Sound and Vibration 145(2): 321-332. DOI: 10.1016/0022-460x(91)90595-b.

Peeters, B., Roeck, G.D. (2001). One-year monitoring of the Z24-Bridge: environmental effects versus damage events. Earthquake Engineering & Structural Dynamics 30:149-171. DOI: 10.1002/1096-9845(200102)30:23.0.CO;2-Z.

Qiao, P., Lu, K., Lestari, W., Wang, J. (2007). Curvature mode shape-based damage detection in composite laminated plates. Composite Structures 80(3): 409-428. DOI: 10.1016/j.compstruct.2006.05.026.

Rezaei, D., Taheri, F. (2009). Experimental validation of a novel structural damage detection method based on empirical mode decomposition. Smart Materials and Structures 18(4): 045004. DOI: 10.1088/0964-1726/18/4/045004.

Salawu, O.S. (1997). Detection of structural damage through changes in frequency: a review. Engineering Structures 19(9): 718-723. DOI: 10.1016/s0141-0296(96)00149-6.

Sampaio, R.P.C., Maia, N.M.M., Silva, J.M.M. (1999). Damage detection using the frequency-response-function curvature method. Journal of Sound and Vibration 226(5): 1029-1042. DOI: 10.1006/jsvi.1999.2340.

Sha, G., Radzieński, M., Cao, M., Ostachowicz, W. (2019). A novel method for single and multiple damage detection in beams using relative natural frequency changes. Mechanical Systems and Signal Processing 132: 335-352. DOI: 10.1016/j.ymssp.2019.06.027.

Shang, Z., Sun, L., Xia, Y., Zhang, W. (2021). Vibration-based damage detection for bridges by deep convolutional denoising autoencoder. Structural Health Monitoring 20(4): 1880-1903. DOI: 10.1177/1475921720942836

Tang, J., Xing, H.Y. (2007). Time delay estimation based on second correlation. Computer Engineering 33: 265-267. DOI: 10.3969/j.issn.1000-3428.2007.21.094. (in Chinese).

Trendafilova, I., Manoach, E. (2008). Vibration-based damage detection in plates by using time series analysis. Mechanical Systems and Signal Processing, 22: 1092-1106. DOI: 10.1016/j.ymssp.2007.11.020.

Wang, F.D., Li, R.P., Xiao, Y.Z., Deng, Q.T., Li, X.B., Song, X.L. (2021). A strain modal flexibility method to multiple slight damage localization combined with a data fusion technique. Measurement 182: 109647. DOI: 10.1016/j.measurement.2021.109647.

Wang, L., Yang, Z., Waters, T. P. (2010). Structural damage detection using cross correlation functions of vibration response. Journal of Sound and Vibration 329(24): 5070-5086. DOI: 10.1016/j.jsv.2010.06.020.

Wang, L., Yang, Z. (2013). Effect of response type and excitation frequency range on the structural damage detection method using correlation functions of vibration responses. Journal of Sound and Vibration 332(4): 645-653. DOI: 10.1016/j.jsv.2012.09.027.

Wang, Z.H., Wu X., Liu, X.Q. (2015). A new noise reduction method for rolling bearing acoustic emission signals based on wavelet packet transformation with quadratic correlation weighted threshold. Journal of Vibration and Shock 34(21): 175-178. (in Chinese).

Yan, W.J., Chronopoulos, D., Yuen, K.V., Zhu, Y.C. (2022). Structural anomaly detection based on probabilistic distance measures of transmissibility function and statistical threshold selection scheme. Mechanical Systems and Signal Processing 162: 108009. DOI: 10.1016/j.ymssp.2021.108009.

Yang, Z., Yu, Z., Sun, H. (2007). On the cross correlation function amplitude vector and its application to structural damage detection. Mechanical Systems and Signal Processing 21(7): 2918-2932. DOI: 10.1016/j.ymssp.2007.03.004.

Yang, Y., Li, J.L., Liang, J.Q., Wang, Y., Zhou, C.H. (2019). Model-free structural damage identification method based on statistical moment theory. Journal of Building Structures 40: 196-204. DOI: 10.14006/j.jzjgxb.2017.0603. (in Chinese).

Zhang, C.W., Mousavi, A.A., Masri, S.F., Gholipour, G., Yan, K., Li, X.L. (2022). Vibration feature extraction using signal processing techniques for structural health monitoring: A review. Mechanical Systems and Signal Processing 177: 109175. DOI: 10.1016/j.ymssp.2022.109175.